# Millimeter-Wave Imaging Radar System Design Based on Detailed System Radar Simulation Tool

Marie Mbeutcha, Giacomo Ulisse, Viktor Krozer

Goethe University Frankfurt, Department of Physics, Terahertz Photonics Group
Frankfurt am Main, Germany
mbeutcha@physik.uni-frankfurt.de

*Abstract*—This paper presents a 35 GHz direct-digital-synthesizer (DDS)-based FMCW radar for future fully-integrated front-end MIMO radar systems with complex signal generation. The full integration of radar front-ends is a challenge at millimeter-wave frequencies due to poor signal integrity and spectrum purity, which are essential for imaging applications. The radar features a Hartley architecture for conversion image rejection in up- and down-conversion and an enhanced push-pull power amplifier architecture for harmonic cancellation. A radar simulation environment has been developed emulating realistic device performance. An innovative 3D electromagnetic propagation model is proposed to account for the antenna and wave propagation to the target. With the above architecture we achieve a conversion image rejection of -53.5 dBc with an output power above 34 dBm across 1 GHz bandwidth, using various commercial components. A spectral purity less than -130 dBc is achieved for the 2nd and 3rd order harmonic suppression, respectively. The total DC consumption is around 30 W determined by the power amplifier.

*Keywords—Frequency-modulated continuous-wave (FMCW) radar, millimeter-wave components, millimeter-wave radar, 3D EM simulation, EM propagation*

## I. INTRODUCTION

The large spectrum availability and the size reduction of components with increasing frequencies have spurred the investigation of high-resolution highly integrated radar front-ends at millimeter-wave (mm-wave) frequencies and beyond [1], [2], [3]. High integration schemes are particularly important in MIMO radar systems, such as those suggested for automotive applications. Heterodyne DDS-based FMCW radar is a good candidate for such systems due to its good sensitivity, selectivity, calibration and the possibility of processing the chirp signal at low frequency [4]. The interferences created by nonlinear elements, especially the image frequency due to mixing, and the harmonics generated by amplifiers with medium to high output power levels, deteriorate signal integrity, which can only be improved with off-chip bandpass filters (BPF).

This paper presents a CAD toolkit for realistic simulation of a 35 GHz DDS-based heterodyne FMCW imaging radar with novel architecture, which considerably improves signal integrity. Section II introduces the transceiver architecture enabling chip integration. Section III describes the simulation method including the modelling of the radar front-end, and a propagation model describing the antennas as well as accurate path propagation to and from the target. The implementation and simulation results are discussed in section IV.
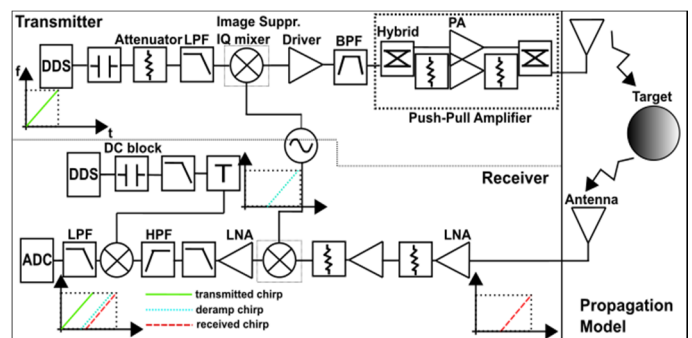


Fig 1. Architecture of the transceiver

## II. SYSTEM DESIGN

Fig. 1 depicts the block diagram of the proposed 35 GHz transceiver system. The transmitter consists of a DDS-based intermediate frequency (IF) signal generation stage, an up-converter stage, and two amplification stages. The up-conversion from IF frequency to mm-wave frequencies is accomplished using synthesized LO signals of phase noise -107 dBc/Hz at 100 kHz. To suppress the resulting strong image frequency, a Hartley architecture is implemented, featuring a sub-harmonic IQ mixer coupled with a 90° hybrid and a single 3rd order BPF filter at the driver output. Finally, to decrease the second harmonic distortion created by the power amplifier operating in saturation, a push-pull amplifier using 180° hybrid couplers is utilized. The push-pull architecture comprises two attenuators to compensate for the gain balance from the couplers [5].

The receiver is composed of two low-noise amplifier stages due to the low power level received from the target and a super-heterodyne down-conversion stage. The down-conversion features an image suppression down-converter in Hartley architecture, followed by a simple down-conversion stage for deramping, where the LO is replaced by a delayed chirp signal generated by a DDS and synchronized with the transmitter [6].
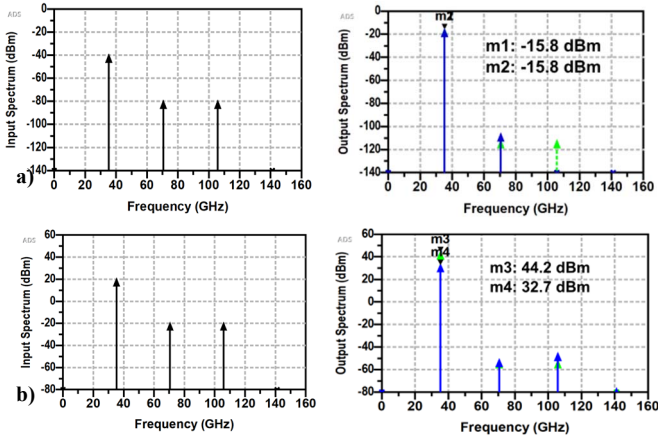
Fig. 2. Frequency characterization of second- and third-order non linearity of PA HMC7229LS6 (dotted green) and emulating component (solid blue) a) in quasi linear mode and b) in saturation. The emulating component shows a saturation at 32.7 dBm and accounts for harmonic distortion and self-mixing.

### III. SIMULATION METHOD

In order to guarantee close-to-reality simulations, each component of the radar front-end has been modelled using parameters from existing commercial devices. In addition, a realistic and novel propagation model is included, comprising the antennas and the full 3D EM propagation simulation to and from the scattering object. This approach enables to predict realistic signals received by the radar and to predict image object quality and resolution.

#### A. Front-end model

Frequency dependent characteristic of the nonlinearity is achieved by cascading a nonlinear block between two linear blocks as described by the Hammerstein-Wiener nonlinear system identification model. The linear blocks are represented by filters. Fig. 2 demonstrates that the emulating component for the power amplifier HMC7229LS6 from Analog Devices [7] accounts for harmonic distortion, gives the correct gain in quasi-linear mode and power saturation properties in large signal input.

The DDS output can be modelled as a quasi-perfect sine wave with low-level spurious signals. This is due to the finite precision in digitally generated sine signals. The spurious-free dynamic range (SFDR) is larger than 50 dBc.

#### B. Propagation model

The simulation of the antenna, the propagation of the transmitted wave and the received wave scattered from the object were performed with a full 3D electromagnetic (EM)
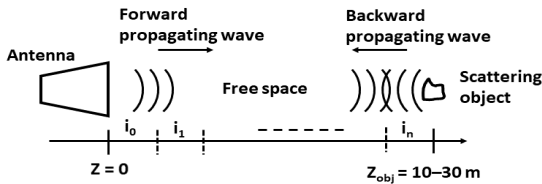


Fig. 3. Simulation scheme

simulation. The 3D EM simulation scheme is shown in Fig. 3. The propagation domain is subdivided into a scattering volume around the Tx and Rx antennas and the object, while the distance to the object is modelled with slabs of pure EM wave propagation. This decomposition results in extremely efficient full-wave simulation of the entire domain and includes consistent simulation of the antenna for the transceiver. The electromagnetic field transmitted from the antenna is exported and used as input in the free space propagation. The free space is divided in N identical sectors as shown in Fig. 3, and the E and H fields for each sector are exported on the interface plane between the free space sectors. With this method, it is possible to simulate the propagation in the forward and backward direction. The EM field after the propagation in the free space is finally imported again in the antenna simulation. This enables the exact calculation of the received signal from the backscattering. The 3D EM simulations were performed with CST Studio using a GPU. This permits to simulate 1 m of free space propagation in about 20 minutes. The full procedure led to the calculation of S-parameters used in transceiver simulations. Fig. 4 reports the amplitude of the transmission coefficient from Tx to Rx. The values are calculated for an object with radar cross-section of $\sigma = 0.01$ m² at 10 m from the antenna. The results are compared with the values calculated with the standard radar equation for an object at 10 m and at 20 m. The 3D EM results fluctuate between the simple radar equation values for 10 m and 20 m. With increasing frequencies, the amplitude rises, which might be due to higher object reflectivity at higher frequencies. The EM simulations provide more realistic results and phase information.
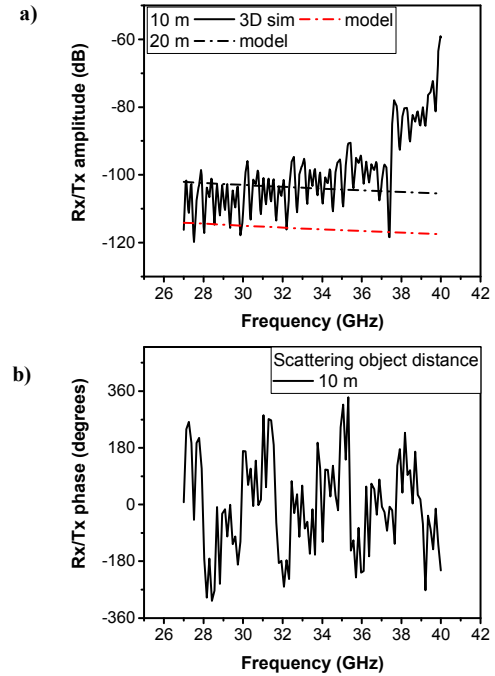


Fig. 4. Ratio between the received and the transmitted signal calculated for a scattering object 10 m and 20 m far from the antenna. a) amplitude, b) phase.
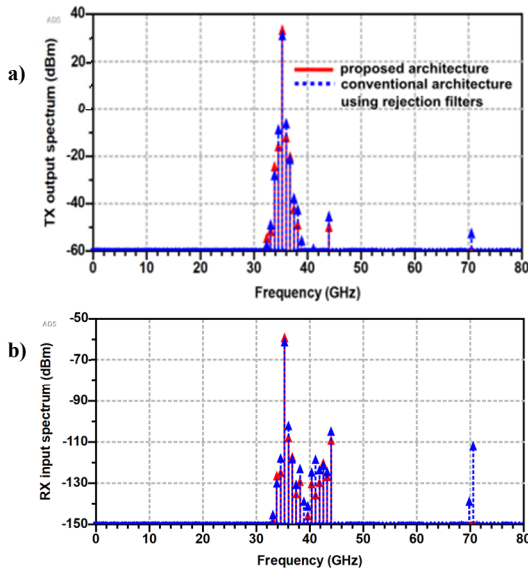
Fig. 5. Spectrum of a) Tx output and b) Rx input using propagation model. There is a rich Tx spectrum below -60 dB. The apparition of harmonics around 40 GHz in the Rx dynamic range is due to the high reflexivity of the target with increasing frequency, unpredictable by the classic radar equation.

The above results for the received and the transmitted signal were included in the global radar simulations as a propagation model.

## IV. SIMULATION RESULTS

The simulation of the radar system was performed with Keysight ADS. A Harmonic Balance simulation provided the results for the output spectrum. In addition, the Envelope simulation was performed to verify the performance of the radar. In each simulation, the propagation model described in Section III.B was included for an object at 10 m and of radar cross section 0.01 m². The antenna gain is 15 dB.

The proposed radar architecture was compared to a conventional radar transceiver using 5th order BPF for image rejection and harmonic cancellation. The results are
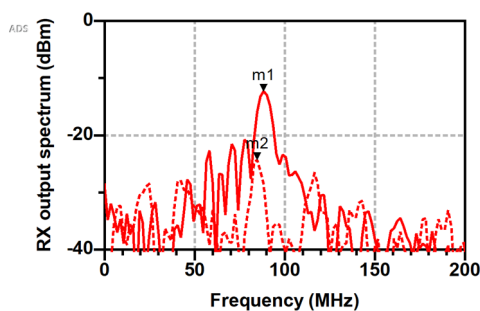


Fig. 6. Rx baseband output spectrum for proposed architecture with radar equation (dotted) and propagation model (solid). NB: the path attenuation is smaller with the propagation model than for the radar equation (cf. Section III.B) hence the greater signal output for the propagation model (m1).

displayed in Fig. 5 and Tab 1. The proposed architecture manages to provide a 34.9 dBm output; this is due to the gain while combining both paths of the enhanced push-pull amplifier. The Hartley and enhanced push-pull architecture combined achieves an in-band SFDR of 45.2 dBc and an out-of-band SFDR of 107.9 dBc which is better than an architecture using image reject filters and facilitates signal integrity. Fig. 6 shows the receiver baseband output spectrum, after deramping. The received signal is clearly showing a single strong reflector with close to Lorentzian shape, testifying of good signal integrity.

TABLE I
OUTPUT INTERFERENCE LEVEL WITH RESPECT TO THE CARRIER

| Frequency | Proposed architecture | Conventional architecture with rejection filters |
|---|---|---|
| Carrier (dBm) | 34.9 | 32.7 |
| LO (dBc) | -45.2 | -38.4 |
| Image (dBc) | -53.5 | -52.7 |
| 2xCarrier (dBc) | -126.5 | -87.5 |
| 3xCarrier (dBc) | -140.5 | -79.4 |
| 10 GHz (dBc) | -107.9 | -104.9 |

## V. CONCLUSION

This paper has investigated a mm-wave FMCW imaging radar in the scope of full front-end integration. The proposed architecture improves signal integrity and guarantees spectral purity. It included two Hartley architectures and an enhanced push-pull amplifier for image and harmonic cancellation, which can be easily integrated on silicon. The radar system operating at 35 GHz showed a spectral purity < -45 dBc in band, and < -100 dBc out of band. The simulation was performed with realistic datasheet-based components and an innovative full 3D electromagnetic simulation was introduced to model the antenna and the path loss to and from the scattering object. This guarantees a close-to-reality simulation environment, essential before implementation.

### REFERENCES

[1] N. Sarmah, J. Grzyb, K. Statnikov, S. Malz, P. Vazquez, W. Förster, B. Heinemann and U. Pfeiffer, "A fully integrated 240 GHz direct-conversion quadrature transmitter and receiver chipset in SiGe technlology," IEEE Transactions on Microwave Theory and Techniques, vol. 64, no. 2, pp. 562-574, 2016.

[2] M. Hitzler, S. Saulig, L. Boehm, W. Mayer, W. Winkler, N. Uddin and C. Waldschmidt, "Ultracompact 160-GHz FMCW radar MMIC," IEEE Transaction on Microwave Theory and Techniques, vol. 65, no. 5, pp. 1682-1691, 2017.

[3]     M. Furqan, F. Ahmed, R. Feger, K. Aufinger and A. Stelzer, "A 120-GHz wideband FMCW radar demonstrator based on a fully-integrated SiGe transceiver with antenna-in-package," in 2016 IEEE MTT-S International Conference on Microwaves for Intelligent Mobility (ICMIM), San Diego, CA, 2016.

[4]     J. Yu, F. Zhao, J. Cali, F. F. Dai, D. Ma, X. Geng, Y. Jin, X. Jin, D. Irwin and R. Jaeger, "An X-band radar transceiver MMIC with bandwidth reduction in 0.13 um SiGe technology," IEEE Journal of Solid-State Circuits, vol. 49, no. 9, September 2014.

[5]     G. Watkins, "Enhancing second harmonic suppression in a ultra-broadband RF push-pull amplifier," High Frequency Electronics, pp. 32-40, March 2014.

[6]     W. Smidth and A. Egido, "Fully focused SAR altimetry: theory and applications," IEEE Transactions on Geoscience and Remote Sensing, vol. 55, no. 1, pp. 392-406, January 2017.

[7]     "HMC7226LS6 datasheet," [Online]. Available: http://www.analog.com [Accessed 3 12 2017].